Available online at www.sciencedirect.com
ScienceDirect
Journal of Sound and Vibration 298 (2006) 918–933
JOURNAL OF SOUND AND VIBRATION
www.elsevier.com/locate/jsvi

Numerical methods for modal analysis of stepped piezoelectric beams

C. Maurini[a], M. Porfiri[b], J. Pouget[a,*]

[a]*Laboratoire de Modélisation en Mécanique, CNRS (UMR7607), Université Pierre et Marie Curie, 4 place Jussieu, 75252 Paris cedex 05, France*

[b]*Department of Mechanical, Aerospace and Manufacturing Engineering, Polytechnic University, Brooklyn, NY 11201, USA*

Received 21 April 2005; received in revised form 17 May 2006; accepted 30 May 2006
Available online 8 August 2006

Abstract

This paper analyzes different numerical methods for modal analysis of stepped piezoelectric beams modeled by the Euler–Bernoulli beam theory. Results from standard numerical approaches, that rely on the discretization of the stepped beam (assumed modes and finite-element methods), are compared with the solution of the exact transcendental eigenvalue problem for the infinite dimensional system. An accurate and manageable novel method, that enriches the assumed modes basis functions with special jump functions, is presented. Numerical results are compared with experimental data and the accuracy of the adopted beam model is validated.
© 2006 Elsevier Ltd. All rights reserved.

1. Introduction

Piezoelectric materials are used as sensors and actuators in control applications because of their ability to simultaneously detect structural deformations and exert control actions in a wide frequency range [1]. Layers of piezoelectric ceramics are integrated in structural elements, by either surface bonding or direct embedding, to form composite electromechanical structures [2–4]. These elements modify the structural properties by adding mass and stiffness, material discontinuities, and new electric properties (such as the equivalent electrical capacitance). Especially in lightweight structures, these additional contributions strongly affect the modal properties of the overall structure and cannot be neglected. At the same time, the precise knowledge of the modal properties is the starting point for controllers design (see e.g. Ref. [5]). For these reasons, many efforts have been devoted to develop numerical and experimental tools for structural modeling of piezoelectric composites.

Galerkin methods, as finite element [6–8] or assumed modes [3,4,9], are frequently used in the modal analysis of stepped piezoelectric beams. They consider a finite-dimensional approximation of the continuum system and reduce the transcendental eigenvalue problem to a linear one. The problem of finding the modal

*Corresponding author. Tel.: +33 0 1 44 27 54 65; fax: +33 0 1 44 27 52 59.
E-mail addresses: maurini@lmm.jussieu.fr (C. Maurini), mporfiri@poly.edu (M. Porfiri), pouget@lmm.jussieu.fr (J. Pouget).

0022-460X/$ - see front matter © 2006 Elsevier Ltd. All rights reserved.
doi:10.1016/j.jsv.2006.05.041

properties of a stepped piezoelectric beam was formulated in Refs. [10–13]. This implies the root-finding of transcendental equations (for natural frequencies) and the inversion of ill-conditioned matrices (for mode shapes). The related numerical problems become soon unsolvable when increasing the number of piezoelectric elements. Accurate methods for the solution of transcendental eigenvalue problems are proposed in Refs. [14,15] (natural frequencies) and in Ref. [16] (natural frequencies and modes shapes), but they have not yet been applied to piezoelectric structures.

In the present paper, we examine and compare four different techniques for modal analysis of stepped piezoelectric beams. The first technique is based on the reliable and efficient method recently proposed in Ref. [16] for the solution of the exact transcendental eigenvalue problem, formulated in terms of the dynamic stiffness matrix (last energy norm (LEN) method). Next, we test, by comparisons with the exact solution from the LEN method, three different Galerkin methods for obtaining a finite-dimensional version of the system. Besides the classical assumed modes (AM) method and finite-element (FE) method, we propose a novel enhanced version of the AM method, which introduces special jump functions (see e.g. Refs. [17,18]) to enrich the standard basis functions (enhanced assumed modes, EAM).

Comparisons between experimental and theoretical results are given in Refs. [7,9,12,19]. However, the accuracy of the numerical techniques used for computing the structural modal properties, on one hand, and the reliability of the experimental methods used for their identification, on the other hand, have not been analyzed thoroughly. For these reasons, it is often difficult to understand if the discrepancies between theoretical predictions and experimental measurements, should be ascribed to inadequate theoretical models, to inaccurate numerical algorithms, to imprecise measurements, or to unreliable identification procedures.

The aims of this paper are manifold: (i) to propose reliable methods to extract modal frequencies and mode shapes of beams with multiple piezoelectric patches; (ii) to comment on the errors introduced by standard approximate methods such as AM and FE, and to suggest possible improvements; (iii) to experimentally show that, for typical materials and geometry, the modal properties of a beam with multiple piezoelectric elements can be reasonably estimated by a simple Euler–Bernoulli model with proper constitutive coefficients.

2. Modeling

The starting point for modeling stepped piezoelectric beams is to choose a suitable one-dimensional (1D) model to describe the interactions between the surface bonded piezoelectric transducers and the host beam. Reviews of the works on beam and plate models of piezoelectric composites can be found in Refs. [1,20,21]. We adopt the Euler–Bernoulli-like model developed in Refs. [22,23]. Its main features are: to introduce the two-fold electromechanical coupling; to include the effect of the induced electric potential [24]; to account for three-dimensional (3D) effects as cross-sectional warping [25]. The corresponding governing equations are in the format of a standard Euler–Bernoulli model, but the constitutive coefficients are improved to get a better agreement with 3D solutions [23].

2.1. Geometry

We consider a beam of length l where two sets of piezoelectric elements are symmetrically bonded side by side to form n_p bimorph pairs. The resulting stepped piezoelectric-composite beam consists of n regular segments. Purely elastic segments alternate with three-layered segments composed of one elastic core and two identical piezoelectric laminae. Each piezoelectric lamina is constituted by piezoelectric ceramics polarized along the thickness direction. Their upper and lower surfaces are covered by two metallic electrodes with negligible mechanical properties. The electrodes of each bimorph pair are connected in parallel and counter-phase in the so-called bender configuration. The generic material point of the beam axis is named by the abscissa x. The generic beam node is indicated by X_h and the generic beam segment of length l_h between X_h and X_{h+1} is indicated by S_h (see Fig. 1). We introduce the subsets of indices I_b and I_p associated to elastic and active piezoelectric segments, respectively.

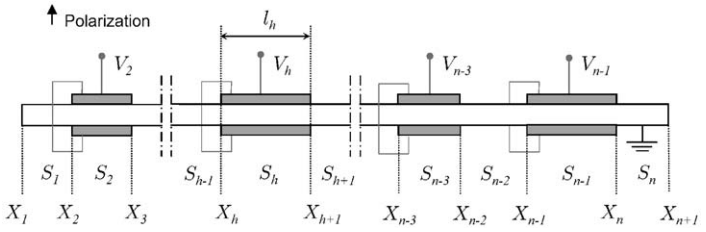

Fig. 1. Sketch of the stepped piezoelectric beam.

2.2. Beam model

The generic segment S_h is modeled as an Euler–Bernoulli beam and its kinematical state at time t is described by the deflection field $w_h(x,t)$ and voltage $V_h(t)$ across the terminals of the bimorph pair (the voltage is defined only if S_h is a piezoelectric segment, i.e. $h \in \mathrm{I}_p$). By assuming a linearized theory, the following constitutive equations relate the bending moment M_h and the line charge density q_h to the bending deformation w_h'' and the voltage V_h (prime denotes the space derivative):

$$M_h(x) = k_h w_h''(x,t) - e_h V_h(t), \tag{1a}$$

$$q_h(x) = e_h w_h''(x,t) + \varepsilon_h V_h(t). \tag{1b}$$

For each piezoelectric segment the mechanical stiffness k_h, the bending coupling coefficient e_h, and the piezoelectric capacitance per unit line ε_h are estimated by the expressions provided in Ref. [23] and reported in Section A.1. For purely elastic segments the constitutive equations (1) reduce to

$$M_h(x,t) = k_h w_h''(x,t). \tag{2}$$

The mechanical equilibrium equation in the generic segment S_h is

$$k_h \frac{\partial^4 w_h(x,t)}{\partial x^4} + \rho_h \ddot{w}_h(x,t) = b(x,t), \tag{3}$$

where ρ_h is the linear mass density, b is the applied transversal load per unit line, and superimposed dot denotes time derivative. The electric equilibrium equations are the Kirchhoff's laws at the n_p ground-referred electric terminals of the piezoelectric segments. At the generic piezoelectric segment S_h, the balance between the total applied electric charge Q_h and the integral of the line charge q_h gives

$$e_h[w_h'(X_{h+1},t) - w_h'(X_h,t)] + C_h V_h(t) = Q_h(t), \tag{4}$$

where $C_h = \varepsilon_h l_h$ is the inherent capacitance (or damped capacitance [6]) of the segment S_h.

The mechanical continuity conditions between different segments imply the continuity of displacement, rotations, shear forces, and bending moment. At node X_h between the segments S_{h-1} and S_h they read

$$\begin{aligned}
&\text{Displacement:} && w_{h-1}(X_h,t) = w_h(X_h,t),\\
&\text{Rotation:} && w_{h-1}'(X_h,t) = w_h'(X_h,t),\\
&\text{Moment:} && k_{h-1} w_{h-1}''(X_h,t) - e_{h-1} V_{h-1}(t) = k_h w_h''(X_h,t) - e_h V_h(t),\\
&\text{Shear:} && k_{h-1} w_{h-1}'''(X_h,t) = k_h w_h'''(X_h,t),
\end{aligned} \tag{5}$$

where the bending moment includes the piezoelectrically induced contribution.[1] For the beam in Fig. 1, the segment S_{h-1} is not piezoelectric and V_{h-1} in Eqs. (5) must be set to zero. The total number of continuity conditions between adjacent segments is $4(n-1)$.

[1]The piezoelectric effect induces a constant bending moment in the piezoelectric segments. This contribution appears only in the continuity conditions. Its effect is equivalent to a pair of opposite bending moments of intensity $e_h V_h$ applied at the ends of each piezoelectric segment.

Eq. (4) shows a well-known result [3,9,26,27]: a piezoelectric sandwich bender is electrically equivalent to a capacitor in parallel connection to a charge generator, whose intensity is proportional to the average curvature of the region covered by the electrodes.

If the potential V_h is imposed by a given voltage source or short-circuited to ground ($V_h = 0$), Eq. (4) is not required for the solution of the problem. If the piezoelectric segment S_h is left open-circuited, then $Q_h(t) = 0$ in Eq. (4) and

$$V_h(t) = -\frac{e_h}{C_h}(w'_h(X_{h+1}, t) - w'_h(X_h, t)). \tag{6}$$

3. Exact formulation

Consider a finite-length beam subject to n_w linear constraints on the deflection fields and their derivatives up to the third order. These constraints include at least four boundary conditions. Moreover, assume that the piezoelectric segments are either short-circuited or open-circuited, and that external forces are null, i.e. $b = 0$. The indices corresponding to closed-circuited segments are collected in the set $\mathrm{I}_p^{\mathrm{SC}}$, those corresponding to open-circuited segments in the set $\mathrm{I}_p^{\mathrm{OC}}$.

By looking for solutions in the harmonic form at frequency ω:

$$w_h(x, t) = \tilde{w}_h(x, \omega)\mathrm{e}^{\mathrm{i}\omega t}, \quad V_h(t) = \tilde{V}_h(\omega)\mathrm{e}^{\mathrm{i}\omega t}, \tag{7}$$

the general solution of the mechanical equilibrium equation of the hth segment is found to be (the dependence on ω is omitted)

$$\tilde{w}_h(x) = a_h \cos\left(\frac{\lambda_h x}{l_h}\right) + b_h \sin\left(\frac{\lambda_h x}{l_h}\right) + c_h \cosh\left(\frac{\lambda_h x}{l_h}\right) + d_h \sinh\left(\frac{\lambda_h x}{l_h}\right), \quad x \in (X_h, X_{h+1}), \tag{8}$$

with

$$\lambda_h = l_h\sqrt{\omega}\sqrt[4]{\frac{\rho_h}{k_h}}. \tag{9}$$

The natural frequencies and mode shapes of the stepped beam are the frequencies ω and the displacement fields in form (8) that verify the n_w constraints and the $4(n-1)$ continuity conditions (5). We introduce the segment nodal displacement vector

$$\mathbf{w}_h = [\tilde{w}_h(X_h) \;\; \tilde{w}'_h(X_h) \;\; \tilde{w}_h(X_{h+1}) \;\; \tilde{w}'_h(X_{h+1})]^{\mathrm{T}} \tag{10}$$

and the segment nodal force vector

$$\mathbf{f}_h = [-\tilde{T}_h(X_h) \;\; -\tilde{M}_h(X_h) \;\; \tilde{T}_h(X_{h+1}) \;\; \tilde{M}_h(X_{h+1})]^{\mathrm{T}}, \tag{11}$$

where $\tilde{M}_h(x)$ and $\tilde{T}_h(x) = -\tilde{M}'_h(x)$ are the harmonic components of bending moment and shear force of the hth segment. The constitutive equations (1) and the expression of the displacement field (8) lead to the following relation between segment nodal forces and segment nodal displacements:

$$\mathbf{f}_h = \mathbf{K}_h\mathbf{w}_h - \mathbf{e}_h\tilde{V}_h, \tag{12}$$

where $\mathbf{K}_h$ is the *segment dynamic stiffness* and $\mathbf{e}_h$ the *segment coupling vector*. The matrix $\mathbf{K}_h$ is given by

$$\mathbf{K}_h = \frac{k_h}{r}\begin{bmatrix} a & -c & f & -d \\ -c & b & d & g \\ f & d & a & c \\ -d & g & c & b \end{bmatrix}. \tag{13}$$

The scalars a, b, c, d, f, g, r are functions of λ_h and l_h:

$$a = -\lambda_h^3(\cosh(\lambda_h)\sin(\lambda_h) + \cos(\lambda_h)\sinh(\lambda_h)), \quad f = \lambda_h^3(\sin(\lambda_h) + \sinh(\lambda_h)),$$

$$b = l_h^2\lambda_h(-\cosh(\lambda_h)\sin(\lambda_h) + \cos(\lambda_h)\sinh(\lambda_h)), \quad g = l_h^2\lambda_h(\sin(\lambda_h) - \sinh(\lambda_h)),$$

$$c = l_h\lambda_h^2\sin(\lambda_h)\sinh(\lambda_h), \quad r = l_h^3(-1 + \cos(\lambda_h)\cosh(\lambda_h)),$$

$$d = l_h^2\lambda_h(\cosh(\lambda_h) - \cos(\lambda_h)). \tag{14}$$

The coupling vector

$$\mathbf{e}_h = [0 \quad -e_h \quad 0 \quad e_h]^{\mathrm{T}} \tag{15}$$

introduces the electrically induced bending moments at the segment ends. For purely elastic segments and short-circuited segments, $\tilde{V}_h = 0$ and Eq. (12) becomes

$$\mathbf{f}_h = \mathbf{K}_h\mathbf{w}_h. \tag{16}$$

Open-circuited segments, for which the voltage is given by Eq. (6), present the stiffening effect due to the open-circuit condition in the modified stiffness matrix:

$$\mathbf{f}_h = \mathbf{K}_h^{\mathrm{open}}\mathbf{w}_h, \quad \mathbf{K}_h^{\mathrm{open}} = \left(\mathbf{K}_h + \frac{1}{C_h}\mathbf{e}_h\mathbf{e}_h^{\mathrm{T}}\right). \tag{17}$$

The global equilibrium equation for null external loading and piezoelectric segments in either short- or open-circuit condition is written in the form

$$\hat{\mathbf{K}}(\omega)\hat{\mathbf{w}} = \mathbf{0}, \tag{18}$$

where $\hat{\mathbf{K}}$ is a $2(n+1)\times 2(n+1)$ *global stiffness matrix* and $\hat{\mathbf{w}}$ is the global nodal displacement vector, comprised of the $2(n+1)$ nodal displacements and rotations. The global stiffness matrix is obtained by assembling the segment matrices of Eqs. (13) and (17) with procedures analogous to those used in FE analysis. When introducing the n_w mechanical constraints, the dynamic stiffness and coupling matrices are modified by eliminating the corresponding degrees of freedom. This leads to the constrained version of Eq. (18)

$$\mathbf{K}(\omega)\mathbf{w} = \mathbf{0}, \tag{19}$$

where $\mathbf{w}$ and $\mathbf{K}(\omega)$ are *constrained* global displacement vector and stiffness matrix.

Eqs. (8) and (19) provide the natural frequencies and mode shapes of a stepped beam with open- or short-circuited piezoelectric segments. Due to the distributed nature of the mechanical system, the characteristic equation (19) is transcendental in ω and finding its roots (natural frequencies) is not trivial. Moreover, whenever a modal frequency is found, standard algorithms generally fail in finding associated mode shapes, because they imply the inversion of ill-conditioned matrices.

The LEN method proposed in Ref. [16] and recalled in Section A.2 provides a reliable method for solving the transcendental eigenvalue problem. It allows for the simultaneous determination of the eigenvalues and the mode shapes without any matrix inversion and with an arbitrary precision. The natural frequencies are computed as the roots of the so-called last energy norm (41) and the corresponding modal nodal displacements by the recursive relations (44).

4. Galerkin methods

Galerkin methods look for approximate solutions of the displacement field of the form [28]

$$w(x,t) = \boldsymbol{\phi}^{\mathrm{T}}(x)\mathbf{y}(t), \tag{20}$$

where $\boldsymbol{\phi}(x)$ and $\mathbf{y}(t)$ are N-dimensional vectors giving a N-dimensional approximation of the deflection field of the stepped beam. The vector $\boldsymbol{\phi}(x)$ collects the basis functions $\phi_i(x)$, and $\mathbf{y}(t)$ the corresponding weighting coefficients $y_i(t)$.

Substituting the Galerkin expansion (20) into an integral formulation of the equations of motion of the stepped beams (3) and (5), leads to a N-dimensional system for the weighting coefficient $\mathbf{y}$. For beams with either open- or short-circuited piezoelectric segments and without mechanical loading, the frequency-domain

version of this system of equations is

$$(-\omega^2\mathbf{M}_G + \mathbf{K}_G)\tilde{\mathbf{y}} = \mathbf{0}, \tag{21}$$

where $\tilde{\mathbf{y}}(\omega)$ is the Fourier transform of $\mathbf{y}(t)$ and mass and stiffness matrices are given by

$$(\mathbf{M}_G)_{ij} = \sum_{h=1}^{n} \rho_h \int_{S_h} \phi_i(x)\phi_j(x)\,\mathrm{d}x, \tag{22}$$

$$(\mathbf{K}_G)_{ij} = \sum_{h=1}^{n} k_h \int_{S_h} \phi_i''(x)\phi_j''(x)\,\mathrm{d}x + \sum_{h\in \mathrm{I}_p^{\mathrm{OC}}} \frac{e_h^2}{C_h}(\phi_i'(X_{h+1}) - \phi_i'(X_h))(\phi_j'(X_{h+1}) - \phi_j'(X_h)). \tag{23}$$

The second contribution to the stiffness matrix in Eq. (23) is the additional stiffness due to the stored electrical energy in open-circuited piezoelectric elements. In this case, the eigenvalue problem is linear in ω^2 and can be easily solved with standard techniques [29]. As the number N of basis functions increases, the solution becomes more accurate [28]. Nevertheless, ad hoc choices of basis functions may lead to fast convergence of the approximate solutions to the exact one. In the following, we present three different methods for generating valuable basis functions.

Here and henceforth, we assume that the basis functions are normalized to satisfy the following condition:

$$\sum_{h=1}^{n} \int_{S_h} \rho_h(\phi(x))^2\,\mathrm{d}x = m, \tag{24}$$

where m is the beam total mass.

4.1. Assumed modes (AM) method

Approximate natural frequencies and mode shapes of stepped piezoelectric beams are often found by considering as basis functions the mode shapes of the corresponding continuous beam without the array of piezoelectric elements (e.g. Refs. [3,9]), i.e. the solutions of

$$\phi^{IV}(\xi) - \lambda^4\phi(\xi) = 0, \quad \lambda = l\sqrt{\omega}\sqrt[4]{\frac{\rho_b}{k_b}}, \quad \xi = \frac{x}{l} \tag{25}$$

with proper mechanical boundary conditions. The resulting basis functions are smooth functions which do not include the curvature discontinuities at the interphase between elastic and piezoelectric segments.

For a cantilever beam the eigenvalues are the roots of the following transcendental equation:

$$1 + \cosh\lambda\cos\lambda = 0. \tag{26}$$

The numerical values for the eigenvalues λ_i and the corresponding mode shapes ϕ_i can be found in several books (see for example Ref. [30]).

4.2. Enhanced assumed modes (EAM) method

A more accurate approximate solution of the eigenvalue problem can be found by enriching the mode shapes of the homogeneous beam with suitable discontinuity functions. These additional functions are tasked with modeling the effects of material discontinuities. Here, we introduce $n-1$ discontinuity functions $\{\theta_h\}_{h=1}^{n-1}$, one for each step between elastic and piezoelectric segments. The generic discontinuity function θ_h is chosen to satisfy the mechanical constraints, to be continuous with its first derivative, and to have a jump on the second derivative at the hth step. A function with these characteristics may be generated as the static deflection of a homogenous beam due to a concentrated bending moment applied at the hth step.

For a left cantilevered beam, the solution of the simple static problem resulting from the application of a concentrated moment at the hth step (i.e. at $x = X_{h+1}$) is

$$\theta_h = \begin{cases} \alpha_h \dfrac{x^2}{2l}, & x \in [0, X_{h+1}), \\ \alpha_h \dfrac{X_{h+1}}{2l}(2x - X_{h+1}), & x \in [X_{h+1}, l]. \end{cases} \tag{27}$$

The constant α_h is proportional to the applied moment and can be chosen in order to normalize the special jump functions as in Eq. (24).

4.3. Finite-element (FE) method

The FE method is a reliable method for the solution of the eigenvalue problem of the stepped piezoelectric beams. We implement the standard two-node 1D FE with quadratic shape functions, which has been employed for a stepped piezoelectric beam in Ref. [6]. The only difference with respect to the model used in Ref. [6] relies on the choice of the constitutive coefficients k_h, e_h, and ε_h of the multilayered piezoelectric segments. Here, these coefficients are estimated through the improved formula presented in Ref. [23] and reported in Eqs. (31). These coefficients intrinsically include 3D effects as cross-sectional warping that are of primary importance in piezoelectric laminates with thickness-polarized piezoelectric layers.

The trial solution in the generic element is constructed from the values of the deflection and rotation at the element nodes (nodal displacements) by using classical Hermite polynomials. In the present case, each beam segment is divided into a number of disjoint elements. The vector of weighting coefficients $\mathbf{y}$ is comprised of the amplitudes of the nodal displacements and rotations at all the mesh nodes. The mass and stiffness matrices of the eth element in the elastic or short-circuited piezoelectric segment S_h are:

$$M_e = \rho_h \begin{bmatrix} \frac{13l_e}{35} & \frac{11l_e^2}{210} & \frac{9l_e}{70} & \frac{-13l_e^2}{420} \\ \frac{11l_e^2}{210} & \frac{l_e^3}{105} & \frac{13l_e^2}{420} & \frac{-l_e^3}{140} \\ \frac{9l_e}{70} & \frac{13l_e^2}{420} & \frac{13l_e}{35} & \frac{-11l_e^2}{210} \\ \frac{-13l_e^2}{420} & \frac{-l_e^3}{140} & \frac{-11l_e^2}{210} & \frac{l_e^3}{105} \end{bmatrix}, \quad K_e = k_h \begin{bmatrix} \frac{12}{l_e^3} & \frac{6}{l_e^2} & \frac{-12}{l_e^3} & \frac{6}{1_e^2} \\ \frac{6}{l_e^2} & \frac{4}{l_e} & \frac{-6}{l_e^2} & \frac{2}{l_e} \\ \frac{-12}{l_e^3} & \frac{-6}{l_e^2} & \frac{12}{l_e^3} & \frac{-6}{l_e^2} \\ \frac{6}{l_e^2} & \frac{2}{l_e} & \frac{-6}{l_e^2} & \frac{4}{l_e} \end{bmatrix}, \tag{28}$$

where l_e is the element length. For elements belonging to open-circuited piezoelectric segments, the stiffness matrix is modified by adding the contribution due to the electrically stored energy

$$\frac{1}{l_e \varepsilon_h} \mathbf{e}_h \mathbf{e}_h^{\mathrm{T}} = \frac{e_h^2}{l_e \varepsilon_h} \begin{bmatrix} 0 & 0 & 0 & 0 \\ 0 & 1 & 0 & 1 \\ 0 & 0 & 0 & 0 \\ 0 & 1 & 0 & 1 \end{bmatrix}, \tag{29}$$

where the coupling vector $\mathbf{e}_h$ is defined by Eq. (15). The global stiffness and mass matrices are computed by assembling the element matrices and by imposing the kinematic constraints.

5. Results

5.1. Experiments

A cantilever aluminum beam (Al6061-T6) hosting two surface bonded bimorph pairs of piezoelectric transducers (Piezo-System T110-H4E-602) was built (see Figs. 2 and 3). Tables 1 and 2 report the corresponding geometric and material properties. This system is a stepped piezoelectric beam composed of five

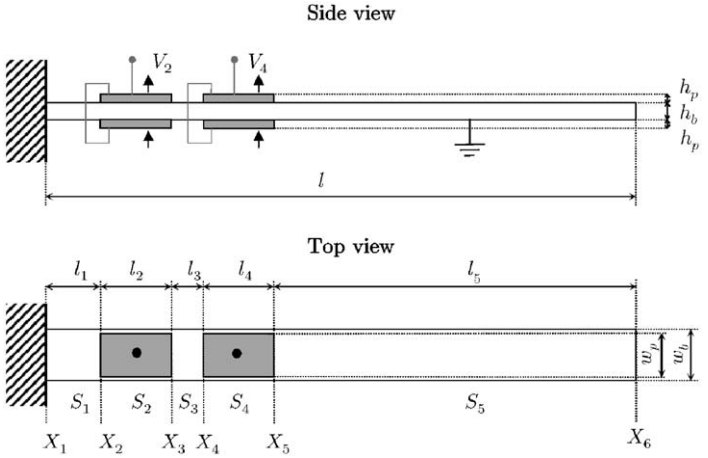

Fig. 2. Geometry of the stepped beam considered in numerical examples and experimental tests. The arrows indicate the polarization of the piezoelectric layers.

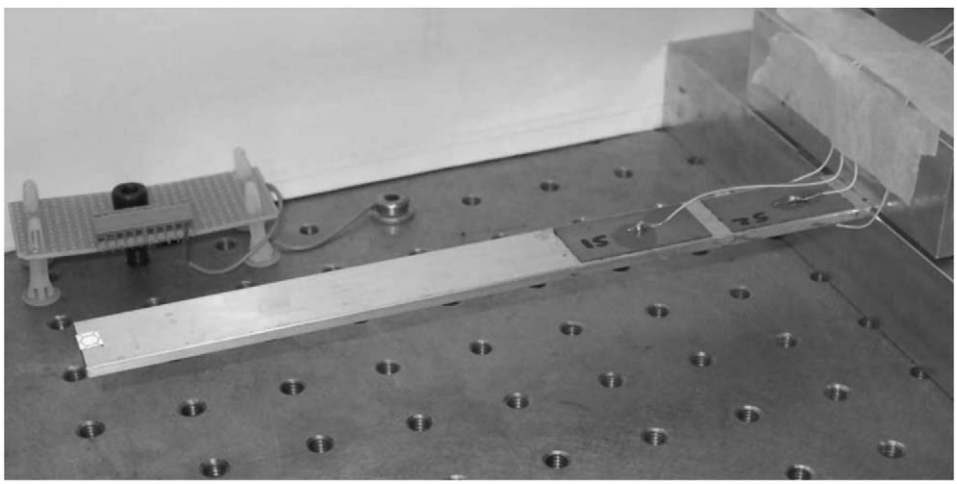

Fig. 3. Picture of the stepped beam used for experimental tests.

Table 1
Dimensions (mm) of the stepped piezoelectric beam

$l_1 = 5.0$,	$l_2 = 36.5$,	$l_3 = 6.0$,	$l_4 = 36.5$,	$l_5 = 117.0$
$l = 201.0$,	$w_p = 17.6$,	$w_b = 20.0$,	$h_p = 0.267$,	$h_b = 2.85$

Table 2
Material data for aluminum and piezoelectric ceramics

Aluminum (*Al6061-T6*)		
$\rho_V^{(\mathrm{al})} = 2700\,\mathrm{kg\,m^{-3}}$,	$Y^{(\mathrm{al})} = 69 \times 10^9\,\mathrm{N\,m^{-2}}$,	$\nu^{(\mathrm{al})} = 0.33$
Piezoelectric ceramics (*PZT-5H-S4-ENH*)		
$\rho_V^{(\mathrm{PZT})} = 7800\,\mathrm{kg\,m^{-3}}$,	$Y_1^{(\mathrm{PZT})} = 62 \times 10^9\,\mathrm{N\,m^{-2}}$,	$Y_3^{(\mathrm{PZT})} = 50 \times 10^9\,\mathrm{N\,m^{-2}}$
$\nu_{12} = 0.31$,	$d_{31} = -320 \times 10^{-3}\,\mathrm{m\,V^{-1}}$,	$d_{33} = 650 \times 10^{-3}\,\mathrm{m\,V^{-1}}$
$\varepsilon_{33}^{\mathrm{T}} = 3800\varepsilon_0$		

regular segments, three elastic and two piezoelectric. The piezoelectric transducers were bonded on the beam by a thin-layer of non-conductive epoxy resin and each bimorph pair was electrically interconnected in parallel and counter-phase. The single piezoelectric transducer is made of a layer of thickness-polarized piezoelectric ceramic (PZT-5H) having the upper and lower surfaces covered by a thin nickel film serving as electrode. The electric contact between the lower electrode of each transducer and the grounded beam was achieved by a small spot of electrically conductive adhesive in the central region of the piezoelectric transducer, where interfacial stresses are low [2].

The beam frequency response was determined by exciting the structure with a frequency sweep signal at one of the two piezoelectric pairs and measuring the beam tip velocity by a laser velocimeter (Polytec OFV 350) as illustrated in Fig. 4. The input signal was generated digitally in Labview, converted by the D/A converter National Instruments AT-MIO-16E-10, and amplified by ad hoc designed voltage amplifier. The analog output of the laser and the voltage applied at the exciting transducer were measured by the A/D converter National Instruments PCI-4452 and a personal computer was used for digital signal processing. Non-invasive measurements were performed by exciting the beam with one of the surface-bonded transducers (included in the model, being part of the stepped beam itself), and by measuring the tip velocity with the laser-vibrometer.

Table 3 reports the measured natural frequencies of the first four structural modes and compares them with the numerical values found by using the LEN method. Fig. 5 displays the experimental and numerical mobility functions obtained either when shunting the first piezoelectric pair and exciting the second one ($V_2 = 0$ and $V_4 = \bar{V}$) or vice versa ($V_2 = \bar{V}$ and $V_4 = 0$). The numerical plots rely on a eight dof modal model obtained by the LEN method.

Table 3 and Fig. 5 assess the accuracy of the simple Euler–Bernoulli model to describe the modal properties of a stepped piezoelectric beam. The difference between the numerical (LEN method) and the experimental values for the first four natural frequencies are within 1.8% error and the frequency responses are barely

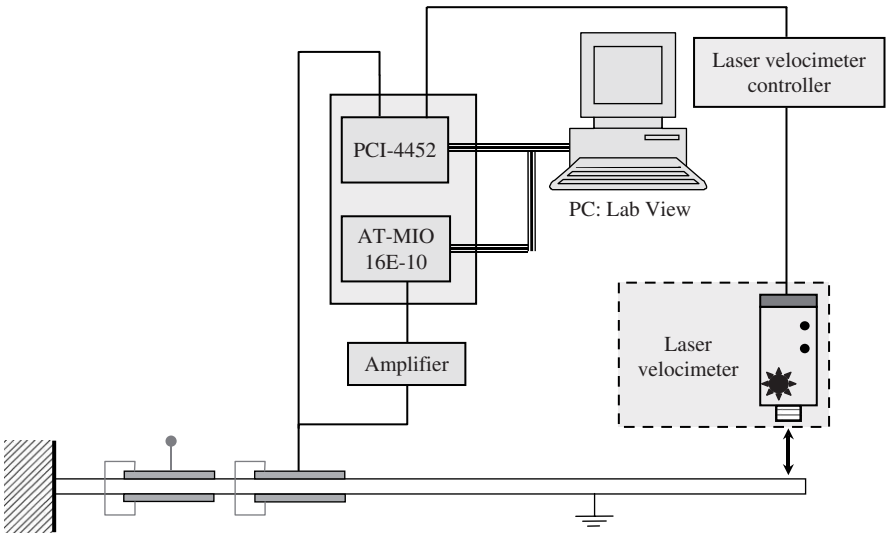

Fig. 4. Experimental setup for frequency response measures.

Table 3
First four natural frequencies of the stepped beam in Figs. 2 and 3 with short-circuited piezoelectric transducers

	f_1 (Hz)	f_2 (Hz)	f_3 (Hz)	f_4 (Hz)
Experimental	66.25	360.2	990	1943
LEN	66.69 (+1.56%)	363.6 (+1.54%)	1001 (+1.79%)	1955 (+1.37%)

Comparisons between experimental values and numerical results of the LEN method.

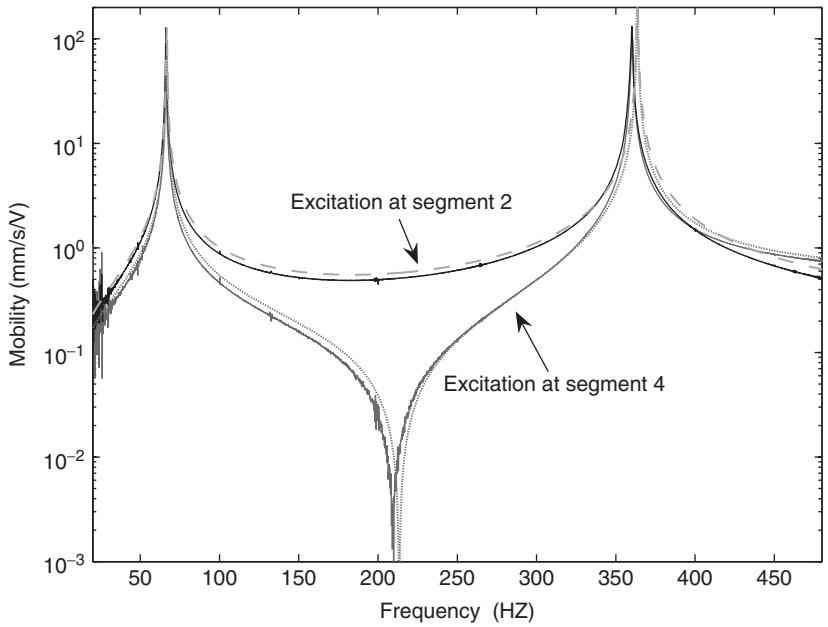

Fig. 5. Experimental mobility function of the stepped beam in Figs. 2 and 3 obtained by applying a frequency sweep at one piezoelectric segment, the other being short-circuited. The response is taken with a velocimeter as in Fig. 4. The different numerical (dashed or dotted lines) and experimental (continuous lines) frequency responses refer to excitation at the second segment ($V_2 = \bar{V}(t)$, $V_4 = 0$) or at the fourth segment ($V_2 = 0$, $V_4 = \bar{V}(t)$).

Table 4
First four natural frequencies of the stepped beam in Figs. 2 and 3 with short-circuited piezoelectric transducers

	f_1 (Hz)	f_2 (Hz)	f_3 (Hz)	f_4 (Hz)
LEN	66.6859	363.590	1001.24	1954.99
AM	67.2832 (+0.89%)	365.742 (+0.592%)	1007.76 (+0.650%)	1969.53 (+0.744%)
EAM	66.6864 ($+6.79 \times 10^{-4}$%)	363.600 ($+2.79 \times 10^{-3}$%)	1001.33 ($+8.25 \times 10^{-3}$%)	1955.19 (+0.0101%)
FE	66.6860 ($+2.12 \times 10^{-4}$%)	363.606 ($+4.24 \times 10^{-3}$%)	1001.49 (+0.0242%)	1957.06 (+0.106%)
Unif. beam	57.6071 (−13.6%)	361.0170 (−0.708%)	1010.86 (+0.960%)	1980.88 (+1.32%)

Comparisons among the results of the different methods including percentile differences with respect to the LEN method. The frequencies of the aluminum beam without the transducers (uniform beam) are reported as reference value.

distinguishable. Moreover, the percentage errors in the first four frequencies are almost constant and the ratios between the natural frequencies are correctly predicted. This validates the Euler–Bernoulli model for low vibration modes and considered geometry and materials. The agreement between theory and experiments also indicates that neglecting shear effects and rotatory inertia is reasonable for thin beams with surface bonded piezoelectric transducers (see also Ref. [12]).

5.2. Comparisons

Table 4 lists the first four natural frequencies for short-circuited piezoelectric elements computed with the four methods above. The corresponding mode shapes and curvatures are plotted in Fig. 6. These results are calculated with the following choices of degrees of freedom: (i) AM method: eight dof given by the first eight mode shapes of the homogeneous cantilever beam; (ii) EAM method: 12 dof, given by the first eight mode

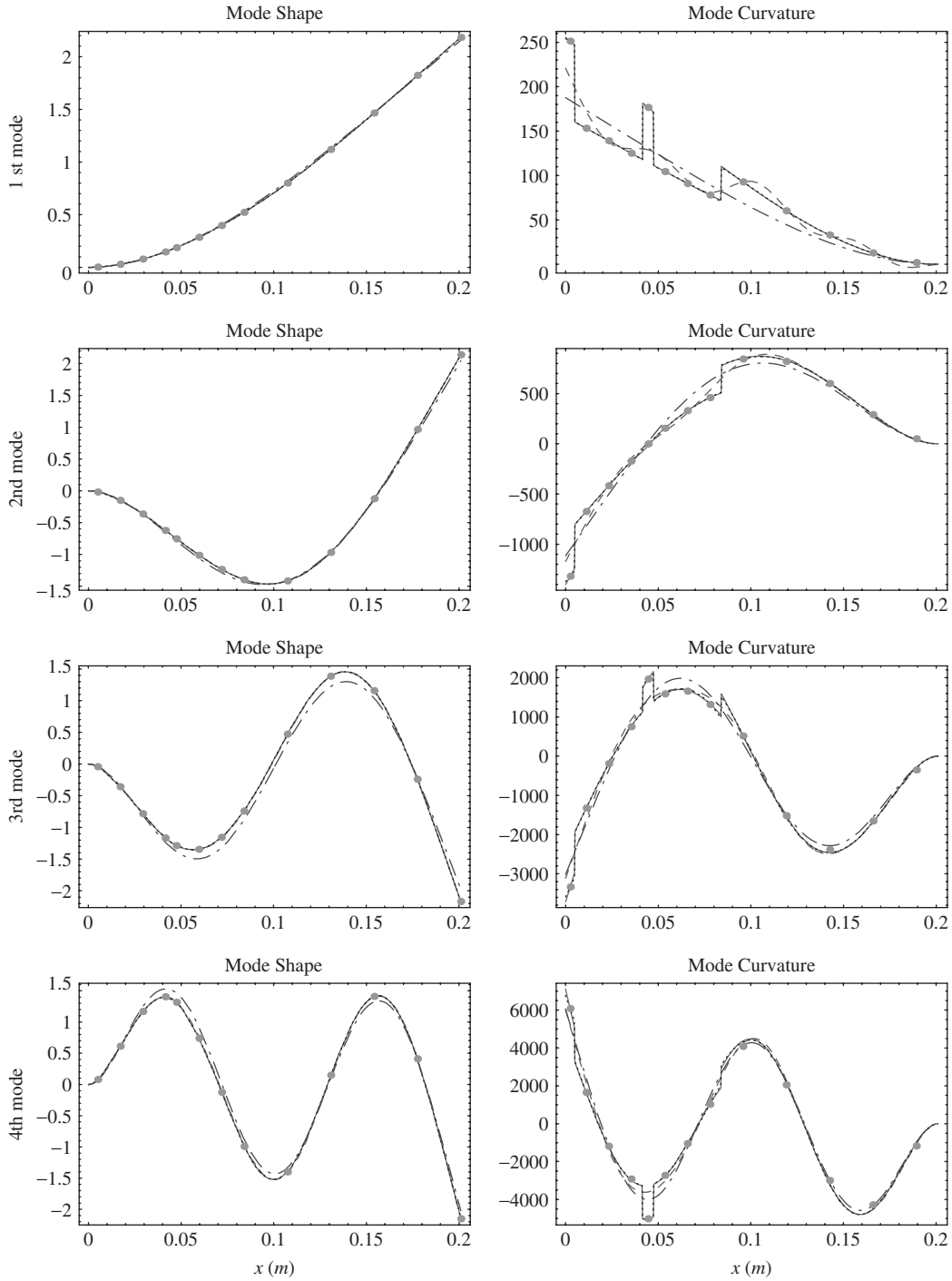

Fig. 6. Mode shapes and mode curvatures of the stepped cantilever beam computed with the presented algorithms (continuous line: LEN; dashed line: AM; dotted line: EAM; dots: FE nodal displacements and average element curvatures; dash-dotted line: modes of the homogenous beam).

shapes of the homogeneous cantilever beam and the 4 jump functions $\{\theta_i\}_{i=1,\ldots,4}$ defined as in Eq. (27); (iii) FE method: 26 dof given by the nodal displacement and rotation at the 13 nodes obtained by subdividing each of the beam segment into subelements of the same length with 1 subelement in the first and third segment,

Table 5
Comparison between the four methods for numerical modal analysis

	LEN	AM	EAM	FE
Accuracy on frequencies	–	Fair	High	High
Accuracy on mode shapes	–	Poor	High	Medium
Basis functions	–	Modes of the hom. beam	Modes of the hom. beam + jump functions	Hermite polynomials
Stiffness matrix	Transcendental, symmetric, banded	Symmetric, not-banded	Symmetric, not-banded	Symmetric, banded
Assembly of matrices	Easy	Not needed	Not needed	Easy
Accuracy on mode curvatures	Very high	Poor	High	High, but requires post-processing

3 subelements in the second and fourth segment, and 5 subelements in the fifth segment. Table 4 also reports the natural frequencies of the homogeneous aluminum beam (without the piezoelectric transducers) to underline the influence of the piezoelectric elements.

Table 5 summarizes the characteristic features of the presented numerical methods. Comparison of the methods suggests the following conclusions:

- The AM, even being the most widespread, does not provide satisfactory determinations of the modal properties. This is due to the excessive smoothness of the basis functions.
- The EAM method provides accurate estimates of the natural frequencies and of the mode shapes because the special jump functions increase the frequencies' accuracies and introduce the effects of the beam segmentation. Its implementation is very easy and it seems to be directly applicable to 2D problems, for example plates and shells hosting piezoelectric transducers (see e.g. Refs. [31,32]).
- The FE method is a well-established method and provides accurate predictions of the natural frequencies. But, even with a larger number of dof, the corresponding estimates of the higher frequencies are worse than those of EAM method. Furthermore, due to the lack of continuity of the curvatures of the basis functions at the element junctions, a satisfactory computation of the mode shapes may require post-processing.
- The LEN method guarantees an arbitrary precision in the computation of the beam modal properties, that may be easily controlled by setting the tolerance of the root-finding algorithm used for the natural frequencies. Its implementation is straightforward, but its extension to 2D problems seems difficult.

6. Conclusions

This paper analyzed numerical methods for modal analysis of stepped piezoelectric beams. The analysis relies on linear models and, for beam modeling, on an Euler–Bernoulli theory including 3D effects [22,23].

Four different numerical techniques have been tested. The exact transcendental eigenvalue problem has been solved by the LEN method [16]. We have proposed a simple and efficient enhancement of classical AM method, that introduces special jump functions to catch the curvature discontinuities of the mode shapes (EAM method). Numerical comparisons have shown that the EAM method may be preferable also to the standard (1D) FE method, especially for higher frequencies.

Comparisons between theoretical and experimental resonance frequencies indicates that an Euler–Bernoulli model correctly predicts the dynamics of a stepped piezoelectric beam with typical geometry and material properties. This is shown by the good agreement between the numerical and experimental natural frequencies and response functions.

Numerical methods established in this paper seem particularly promising in analyzing and designing distributed control systems similar to those proposed in Refs. [4,26,27], where arrays of piezoelectric elements

and distributed electric circuits are exploited for multimodal vibration damping. Further extensions of the present work should address the problem of an accurate numerical modal analysis of plates with multiple piezoelectric patches, as those considered in Refs. [31,32].

Acknowledgments

The present work has been done in the framework of the joint research project "Smart materials and structures: structural control using distributed piezoelectric transducers and passive electric networks" funded by the international agreement between CNRS (France) and CNR (Italy), project n.16283. The authors would also like to acknowledge Prof. A. Sestieri for the comments on a preliminary version of the manuscript and for offering them access to the experimental facilities of the Mechanical Vibrations Laboratory of the University of Rome "La Sapienza", where the experiments have been performed.

Appendix A

A.1. Constitutive parameters of a stepped piezoelectric beam

The coefficients appearing in the electromechanical constitutive relations of the three-layer sandwich piezoelectric beam with counter-phase connected piezoelectric layers, can be estimated with different modeling approaches. As shown in Refs. [22,23], standard models assuming an uniaxial stress state lead to relevant errors in estimating the equivalent piezoelectric capacitance. Here, the coefficients found by the null transverse stress resultants model proposed in Ref. [23] are used. The beam constitutive coefficients are found from the beam cross-sectional geometry and the following constitutive parameters: $Y_1^{(\mathrm{PZT})}$, ν_{12} (in-plane Young modulus and Poisson ratio of the piezoelectric material at constant electric field), d_{31} (piezoelectric strain coefficient), $\varepsilon_{33}^{\mathrm{T}}$ (dielectric permittivity at constant stress along the direction of polarization), Y and ν (host beam Young modulus and Poisson ratio).

In standard IEEE notation [33], we define the plane stress ($T_{33}=0$) coefficients

$$\tilde{c}_{11}^{E}=\frac{Y_1^{(\mathrm{PZT})}}{1-\nu_{12}^2},\quad \tilde{c}_{12}^{E}=\nu_{12}\frac{Y_1^{(\mathrm{PZT})}}{1-\nu_{12}^2}, \tag{30a}$$

$$\tilde{e}_{31}=-d_{31}\frac{Y_1^{(\mathrm{PZT})}}{1-\nu_{12}},\quad \tilde{\varepsilon}_{33}^{S}=\varepsilon_{33}^{\mathrm{T}}-2d_{31}^2\frac{Y_1^{(\mathrm{PZT})}}{1-\nu_{12}}, \tag{30b}$$

$$\tilde{c}_{11}^{D}=\tilde{c}_{11}^{E}+\tilde{e}_{31}^2/\tilde{\varepsilon}_{33}^{S},\quad \tilde{c}_{12}^{D}=\tilde{c}_{12}^{E}+\tilde{e}_{31}^2/\tilde{\varepsilon}_{33}^{S}, \tag{30c}$$

$$\tilde{c}_{11}=\frac{Y}{1-\nu^2},\quad \tilde{c}_{12}=\nu\frac{Y}{1-\nu^2}. \tag{30d}$$

Using Eq. (30), the constitutive coefficients for the hth segment (piezoelectric), under the conditions of vanishing transversal force resultants, are calculated as [23]:

$$k_h=a_bK_{11}\left(1-\frac{K_{12}^2}{K_{11}^2}\right)+(a_p-a_b)\frac{1}{12}h_b^3\tilde{c}_{11}(1-\nu^2), \tag{31a}$$

$$e_h=a_b\tilde{e}_{31}(h_p+h_b)\left(1-\frac{K_{12}}{K_{11}}\right), \tag{31b}$$

$$\varepsilon_h=\frac{2a_p\tilde{\varepsilon}_{33}^{S}}{h_p}+\frac{(a_p\tilde{e}_{31}(h_p+h_b))^2}{K_{11}}, \tag{31c}$$

where the stiffness parameters K_{11}, K_{12} are defined by

$$K_{\alpha\beta} = \frac{\tilde{c}^E_{\alpha\beta} h_p^3}{12}\left(6\left(1+\frac{h_b}{h_p}\right)^2 + 2\frac{\tilde{c}^D_{\alpha\beta}}{\tilde{c}^E_{\alpha\beta}} + \frac{\tilde{c}_{\alpha\beta}}{\tilde{c}^E_{\alpha\beta}}\frac{h_b^3}{h_p^3}\right). \tag{32}$$

The linear mass density ρ_h is given by

$$\rho_h = a_b h_b \rho_V \tag{33}$$

in purely elastic segments, and by

$$\rho_h = a_b h_b \rho_V + 2 a_p h_p \rho_V^{(\mathrm{PZT})} \tag{34}$$

in piezoelectric segments. The parameters ρ_V and $\rho_V^{(\mathrm{PZT})}$ are the volume mass density of the elastic and piezoelectric materials.

For the geometrical and material data reported in Tables 1 and 2, numerical values of the constitutive coefficients (31)–(34) are

$$\text{piezoelectric segment:} \begin{cases} k_h = 4.099\,\mathrm{N\,m^2}, \\ \rho_h = 0.2280\,\mathrm{kg\,m^{-1}}, \\ \varepsilon_h = 2.6252\times 10^{-6}\,\mathrm{F\,m^{-1}}, \\ e_h = -0.00108\,\mathrm{N\,m\,V^{-1}}, \end{cases} \tag{35}$$

$$\text{elastic segment:} \begin{cases} k_h = 2.662\,\mathrm{N\,m^2}, \\ \rho_h = 0.1539\,\mathrm{kg\,m^{-1}}. \end{cases} \tag{36}$$

A.2. Solution of the transcendental eigenvalue problem

We briefly review the procedure presented in Ref. [16] (and called in the present paper LEN method) for solving the transcendental eigenvalue problem for a structure consisting of n continuous substructures:

$$\mathbf{K}(\omega)\mathbf{x} = \mathbf{0}, \tag{37}$$

where $\mathbf{K}$ is a $n \times n$ real symmetric, non-negative definite dynamic stiffness matrix whose entries are transcendental functions of ω. At any trial frequency $\bar{\omega}$ the symmetric matrix $\mathbf{K}$ can be decomposed in terms of a non-singular lower triangular matrix $\mathbf{L}$ with unit diagonal elements and a diagonal matrix $\mathbf{D}$:

$$\mathbf{K} = \mathbf{L}\mathbf{D}\mathbf{L}^{\mathrm{T}}. \tag{38}$$

Or equivalently,

$$\mathbf{P}^{\mathrm{T}}\mathbf{K}\mathbf{P} = \mathbf{D}, \tag{39}$$

where the upper triangular matrix $\mathbf{P}$, satisfying

$$\mathbf{P} = \mathbf{L}^{-\mathrm{T}} \tag{40}$$

is introduced. The last entry of $\mathbf{D}$ is called last energy norm (LEN) and it is given by

$$d_n = \mathbf{P}_n^{\mathrm{T}}\mathbf{K}\mathbf{P}_n, \tag{41}$$

where the matrix subscript n indicates the nth column, thus $\mathbf{P}_n$ is the last column vector of $\mathbf{P}$. From Eqs. (38) and (40) we find:

$$\mathbf{K}\mathbf{P}_n = (\mathbf{K}\mathbf{P})_n = (\mathbf{L}\mathbf{D})_n. \tag{42}$$

By noticing that $\mathbf{L}$ is lower triangular with unit diagonal elements and $\mathbf{D}$ is diagonal, we obtain

$$\mathbf{K}\mathbf{P}_n = d_n \mathbf{I}_n, \tag{43}$$

where $\mathbf{I}$ is the n-dimensional identity matrix. Therefore, if d_n vanishes at $\bar{\omega}$, then $\bar{\omega}$ is a natural frequency and $\mathbf{P}_n$ is the corresponding eigenvector, which can be found from the following recursive relations:

$$\mathbf{P}_1 = \mathbf{I}_1, \quad \mathbf{F}_1 = (\mathbf{K})_1,$$

$$\mathbf{P}_k = \mathbf{I}_k - \sum_{i=1}^{k-1} \frac{(\mathbf{F}_k)_i}{(\mathbf{F}_i)_i} \mathbf{P}_i, \quad \mathbf{F}_k = (\mathbf{K})_k - \sum_{i=1}^{k-1} \frac{(\mathbf{F}_k)_i}{(\mathbf{F}_i)_i} \mathbf{F}_i, \tag{44}$$

where $\mathbf{F}$ is a lower triangular matrix defined by

$$\mathbf{F} = \mathbf{P}^{-\mathrm{T}}\mathbf{D} = \mathbf{K}\mathbf{P}. \tag{45}$$

In this way, the eigenvalues are obtained as the root of the LEN d_n and the associated eigenvectors are simultaneously found, without any matrix inversion, as the corresponding $\mathbf{P}_n$. Moreover, it is possible to show [16] that d_n is a monotonically decreasing function of the frequency ω and its graph is composed of infinite branches separated by singular points where the function is approaching $-\infty$ from the left and $+\infty$ from the right. Therefore, for each branch there is a unique root of d_n which can be easily found by applying standard root-searching algorithms (e.g. bisection).

The problem of properly locating each eigenvalue, meaning giving suitable upper and lower bounds on any specific eigenvalue, can be solved by using the Wittrick–Williams *mode count function* [15]

$$J(\bar{\omega}) = \sum_{k=1}^{n} J_k(\bar{\omega}) + s(\mathbf{K}(\bar{\omega})). \tag{46}$$

Eq. (46) yields the number J of natural frequencies that are exceeded by a trial frequency $\bar{\omega}$. The term J_k in Eq. (46) is the number of natural frequencies of the kth substructure that would be exceeded by $\bar{\omega}$ if its ends were to be clamped (i.e. the nodal displacements set to zero). For Euler–Bernoulli beams a simple formula for J_k may be derived (see Ref. [14]):

$$J_k = j - \tfrac{1}{2}(1 - (-1)^j \operatorname{sign}(1 - \cosh\lambda_k \cos\lambda_k)), \tag{47}$$

where λ_k is defined in Eq. (9), j is the largest integer less than λ_k/π and the function sign gives the argument sign. The term $s(\mathbf{K}(\bar{\omega}))$ is the so-called *sign count* of the symmetric matrix $\mathbf{K}$, and equals the number of negative elements along the diagonal of $\mathbf{D}$.

With this procedure only the eigenvalues related to eigenvectors having zero displacement for the last node are missed [16]. Indeed, by assuming that $\bar{\mathbf{v}}$ is the eigenvector associated to $\bar{\omega}$ and that $d_n(\bar{\omega}) \neq 0$, from decomposition (38)

$$0 = (\mathbf{K}\bar{\mathbf{v}})_n = d_n(\bar{\mathbf{v}})_n. \tag{48}$$

Eq. (48) implies that the nodal displacement $(\bar{\mathbf{v}})_n$ vanishes. In Ref. [16] it is shown that these particular eigenvalues can be determined by re-numbering nodes on the structure or by suitably adding nodes.

References

[1] I. Chopra, Review of state of art of smart structures and integrated systems, *AIAA Journal* 40 (2002) 2145–2187.

[2] E.F. Crawley, J. de Luis, Use of piezoelectric actuators as elements of intelligent structures, *AIAA Journal* 25 (1987) 1373–1385.

[3] N.W. Hagood, A. von Flotow, Damping of structural vibrations with piezoelectric materials and passive electrical networks, *Journal of Sound and Vibration* 146 (1991) 243–268.

[4] F. dell'Isola, C. Maurini, M. Porfiri, Passive damping of beam vibrations through distributed electric networks and piezoelectric transducers: prototype design and experimental validation, *Smart Materials and Structures* 13 (2004) 299–308.

[5] K. Zhou, J. Doyle, K. Glover, *Robust and Optimal Control*, Prentice-Hall, New Jersey, 1996.

[6] Y. Kagawa, G.L.M. Gladwell, Finite element analysis of flexure-type vibrators with electrostrictive transducers, *IEEE Transactions on Sonics and Ultrasonics* 17 (1970) 41–49.

[7] Z.K. Kusculuoglu, B. Fallahi, T.J. Royston, Finite element model of a beam with a piezoceramic patch actuator, *Journal of Sound and Vibration* 276 (2004) 27–44.

[8] C.C. Lin, H.N. Huang, Vibration control of beam-plates with bonded piezoelectric sensor and actuators, *Computers and Structures* 73 (1999) 239–248.

[9] C.H. Park, Dynamics modelling of beams with shunted piezoelectric elements, *Journal of Sound and Vibration* 268 (2003) 115–129.
[10] S.M. Yang, Y.J. Lee, Modal analysis of stepped beams with piezoelectric materials, *Journal of Sound and Vibration* 176 (1994) 289–300.
[11] S.M. Yang, Y.J. Lee, Interaction of structure vibration and piezoelectric actuation, *Smart Materials and Structures* 3 (1994) 494–500.
[12] N.D. Maxwell, S.F. Asokanthan, Modal characteristics of a flexible beam with multiple distributed actuators, *Journal of Sound and Vibration* 269 (2004) 19–31.
[13] U. Lee, J. Kim, J. Shin, A.Y.T. Leung, Development of a Wittrick–Williams algorithm for the spectral element model of elastic-piezoelectric two-layer active beams, *International Journal of Mechanical Sciences* 44 (2002) 305–318.
[14] W.H. Wittrick, F.W. Williams, An automatic computational procedure for calculating natural frequencies of skeletal structures, *International Journal of Mechanical Sciences* 12 (1970) 781–791.
[15] W.H. Wittrick, F.W. Williams, A general algorithm for computing natural frequencies of elastic structures, *Quarterly Journal of Mechanics and Applied Mathematics* 24 (1971) 263–284.
[16] Q. Zhaohui, D. Kennedy, F.W. Williams, An accurate method for transcendental eigenproblems with a new criterion for eigenfrequencies, *International Journal of Solids and Structures* 41 (2004) 3225–3242.
[17] R.C. Batra, M. Porfiri, D. Spinello, Treatment of material discontinuity in two Meshless Local Petrov–Galerkin (MLPG) formulations of axisymmetric transient heat conduction, *International Journal for Numerical Methods in Engineering* 61 (2004) 2461–2479.
[18] R.C. Batra, M. Porfiri, D. Spinello, Free and forced vibrations of a segmented bar by a meshless local Petrov–Galerkin MPLG formulation, *Computational Mechanics*, in press, DOI:10.007/s00466-006-00496-6.
[19] N. Zhang, I. Kirpitchenko, Modelling the dynamics of a continuous structure with a piezoelectric sensor/actuator for passive structural control, *Journal of Sound and Vibration* 249 (2002) 251–261.
[20] D.A. Saravanos, P.R. Heyliger, Mechanics and computational models for laminated piezoelectric beams, plates, and shells, *Applied Mechanics Review* 52 (1996) 305–320.
[21] S.V. Gopinathan, V.V. Varadan, V.K. Varadan, A review and critique of theories for piezoelectric laminates, *Smart Materials and Structures* 9 (2000) 24–48.
[22] C. Maurini, J. Pouget, F. dell'Isola, On a model of layered piezoelectric beams including transverse stress effect, *International Journal of Solids and Structures* 41 (2004) 4473–4502.
[23] C. Maurini, J. Pouget, F. dell'Isola, Extension of the Euler–Bernoulli model of piezoelectric laminates to include 3D effects via a mixed approach, *Computers and Structures* 84 (2006) 1438–1458.
[24] K.Y. Sze, X.M. Yang, H. Fan, Electric assumptions for piezoelectric laminate analysis, *International Journal of Solids and Structures* 41 (2004) 2363–2382.
[25] W. Beckert, G. Pfundtner, Analysis of the deformational behaviour of a bimorph configuration with piezoelectric actuation, *Smart Materials and Structures* 11 (2002) 599–609.
[26] C. Maurini, F. dell'Isola, D. Del Vescovo, Comparison of piezoelectronic networks acting as distributed vibration absorbers, *Mechanical Systems and Signal Processing* 18 (2004) 1243–1271.
[27] U. Andreaus, F. dell'Isola, M. Porfiri, Piezoelectric passive distributed controllers for beam flexural vibrations, *Journal of Vibration and Control* 10 (2004) 625–659.
[28] L. Meirovitch, *Elements of Vibration Analysis*, McGraw-Hill, New York, 1986.
[29] W.H. Press, B.P. Flannery, S.A. Teukolsky, W.T. Vetterling, *Numerical Recipes in Fortran*, Cambridge University Press, Cambridge, 1992.
[30] R.D. Blevins, *Formulas for Natural Frequency and Mode Shape*, Krieger, Malabar, 1995.
[31] S. Alessandroni, U. Andreaus, F. dell'Isola, M. Porfiri, Piezo-electromechanical (PEM) Kirchhoff–Love plates, *European Journal of Mechanics—A/Solids* 23 (2004) 689–702.
[32] S. Alessandroni, U. Andreaus, F. dell'Isola, M. Porfiri, A passive electric controller for multimodal vibrations of thin plates, *Computers and Structures* 83 (2005) 1236–1250.
[33] ANSI/IEEE std 176-1987, IEEE Standard on Piezoelectricity, 1988.